Journal of Alloys and Compounds 509 (2011) 590–595

Contents lists available at ScienceDirect

Journal of Alloys and Compounds

journal homepage: www.elsevier.com/locate/jallcom

Synthesis of calcium alanate and its dehydriding performance enhanced by FeF_3 doping

Changxu Li, Xuezhang Xiao, Lixin Chen*, Kun Jiang, Shouquan Li, Qidong Wang

Department of Materials Science and Engineering, Zhejiang University, Hangzhou 310027, People's Republic of China

ARTICLE INFO

Article history:
Received 14 July 2010
Received in revised form 25 August 2010
Accepted 7 September 2010
Available online 20 October 2010

Keywords:
Calcium alanate
Dehydriding performance
Iron fluoride
Ball-milling

ABSTRACT

$Ca(AlH_4)_2$ was synthesized by ball-milling the mixture of $NaAlH_4$ and $CaCl_2$ in a molar ratio of 2:1 and under a hydrogen atmosphere of 1 MPa. The results indicate that the reactants have entirely transformed to $Ca(AlH_4)_2$ with a byproduct of NaCl after ball-milling for 48 h. Investigations of dehydriding behavior of the as-prepared $Ca(AlH_4)_2$ sample show that approximately 5.2 wt.% of hydrogen is desorbed during the first two dehydrogenation reactions of $Ca(AlH_4)_2$, which exhibit an exothermic event at 148 °C and an endothermic event at 267 °C, respectively. The high temperature dehydrogenation at 267 °C mainly concentrates on the thermolysis of $CaAlH_5$ intermediate. FeF_3-doped $Ca(AlH_4)_2$ system represents an improved dehydriding performance, the dehydrogenation temperature of $CaAlH_5$ intermediate is decreased about 43 °C. After FeF_3 doping, the apparent activation energy of $CaAlH_5$ is reduced from 153.4 kJ/mol (undoped) to 88.3 kJ/mol (doped), it renders a possibility to realize the rehydrogenation of $CaAlH_5$. The catalytic effect is attributed to a fluorine transfer reaction that occurred to generate CaF_2 and Fe catalysts.

1. Introduction

Great efforts have being paid to find an efficient means of storing hydrogen as a fuel on board, but there is still a long way between the targeted and currently available technologies. Since Bogdanovic and Schwickardi [1] discovered that sodium alanate doped with Ti could be reversibly dehydrogenated and rehydrogenated, alanates became one of the most promising hydrogen storage materials, generally characterized by high hydrogen capacity and less than perfect thermodynamic and kinetic properties [2–5]. Current studies have extended to alternative complex hydride systems in order to clarify the hydrogen absorption/desorption mechanism and screen for potential materials of more practical value [6–7]. $LiAlH_4$ has a theoretical capacity of 10.6 wt.% H_2, the direct hydrogenation of $LiAlH_4$ is difficult to be achieved because of its unstable thermodynamics. The decomposition of $KAlH_4$ occurs through three endothermic events at temperatures of 294, 311, and 347 °C with the release of 3.8 wt.% hydrogen, and its catalyzed sample exhibits dehydrogenation temperatures dropped by nearly 50 °C, however, which are still rather high when compared to sodium and lithium alanates [8]. $Ca(AlH_4)_2$ with a total hydrogen capacity of 7.9 wt.% has been far less studied. Its decomposition process mainly consists of four-step reactions, of which the first two steps with the release of 5.9 wt.% hydrogen can be considered for practical applications [9].

$$Ca(AlH_4)_2 \rightarrow CaAlH_5 + Al + 3/2H_2 \quad (1)$$

$$CaAlH_5 \rightarrow CaH_2 + Al + 3/2H_2 \quad (2)$$

$$CaH_2 + 4Al \rightarrow Al_4Ca + H_2 \quad (3)$$

$$CaH_2 + Al_4Ca \rightarrow 2Al_2Ca + H_2 \quad (4)$$

Calcium alanate was first synthesized with CaH_2 and $AlCl_3$ in THF in the 1950s, mainly used as a reducing agent for a long time [10]. Later works about the synthesis of calcium alanate went through a metathesis reaction of $CaCl_2$ and $NaAlH_4$ by wet-chemical or mechanochemistry method, thermal dissociation process as well as thermodynamic and kinetic properties of $Ca(AlH_4)_2$ were also illustrated [11–13]. Recently, Kabbour et al. [14] reported a direct synthesis path of $Ca(AlH_4)_2$ by ball-milling the mixture of AlH_3 and CaH_2. Besides, it was reported that $CaAlH_5$ as an important intermediate could also be synthesized by using AlH_3 and CaH_2 [15]. However, the preparation of AlH_3 is still a challenge. Another way of preparing alkaline earth alanates through hydrogenation of alkaline earth-Al alloy was proved to be invalid for $Ca(AlH_4)_2$ as well as $Mg(AlH_4)_2$, in despite of its feasibility in forming Sr_2AlH_7 and Ba_2AlH_7 [16,17]. The structural properties of $Ca(AlH_4)_2$ and $CaAlH_5$ have been determined by first-principle density function theory (DFT) calculation in the past few years. Crystal structure of $Ca(AlH_4)_2$ is confirmed to be CaB_2F_8-type and that of $CaAlH_5$ consists of corner sharing $[AlH_6]$ octahedral that form heli-

* Corresponding author. Tel.: +86 571 8795 1152; fax: +86 571 8795 1152.
E-mail address: lxchen@zju.edu.cn (L. Chen).

0925-8388/$ – see front matter © 2010 Elsevier B.V. All rights reserved.
doi:10.1016/j.jallcom.2010.09.155

cal chains [18–21]. From the foregoing, attempts to improve the properties of $Ca(AlH_4)_2$ and $CaAlH_5$, such as doping or element substitute, are also important. Better understanding of $Ca(AlH_4)_2$ system renders an important perspective to investigate other complex hydrides with high capacity.

In this work, we attempt to illustrate the synthetic process and catalytic modification of $Ca(AlH_4)_2$. Furthermore, the effect of FeF_3-doping on the dehydriding properties of $Ca(AlH_4)_2$ has been investigated in an attempt to understand the role played by FeF_3 catalyst on the enhancement of the dehydriding properties.

2. Experiments

Synthesis operations of $Ca(AlH_4)_2$ sample were conducted using commercial $NaAlH_4$ (with purity ≥90%, Aldrich) and $CaCl_2$ (with purity ≥96%, Alpha Aesar) that were used without further purification. To prevent any contamination, whole synthesis process was done in a glovebox filled with high pure argon atmosphere (99.999% purity) with the content of water and oxygen below 5 ppm. Prior to milling, $NaAlH_4$ and $CaCl_2$ were mixed in a molar ratio of 2:1 according to the reaction: $[2NaAlH_4 + CaCl_2 \rightarrow Ca(AlH_4)_2 + 2NaCl]$ with a total sample amount of 2.74 g. The mixture was transferred into a sealed stainless steel vial equipped with a gas valve, under 1 MPa of pure hydrogen atmosphere. The ball to powder ratio was about 40:1. Milling was carried out on a planetary ball mill (QM-3SP4, Nanjing) at 400 rpm with different milling time. Every 0.4 h a pause (0.1 h) was set to counterbalance the temperature rise during milling. The sample of 10 wt.% FeF_3-doped calcium alanate was prepared by milling FeF_3 (with purity ≥98%, Aldrich) and the synthetic product (previously milled for 48 h) for 3 h under 0.5 MPa hydrogen pressure with ball to powder ratio of 60:1, the milling rate was reduced to 200 rpm to prevent the untimely dissociation.

Structural characterization was determined by a Rikagu D/Max-RA X-ray diffractometer with Cu Kα radiation at 40 kV and 30 mA from 10° to 90° (2θ) with step increments of 0.05°, a homemade container filled with argon was used to prevent the samples against contamination. IR spectrum of the sample was recorded in the range of 400–4000 cm^{-1} at ambient condition in air using a Bruker Tensor 27 FTIR spectrometer. The dehydriding processes of the samples were carried out on a calibrated Sievert's type apparatus, details are described in the results part. For the differential scanning calorimetry and thermogravimetric (DSC/TG), measurements were conducted on a Netasch DSC 449F3 at different heating rate from 30 to 450 °C. X-ray photoelectron spectroscopy (XPS) was used to monitor the change of FeF_3 phase during the catalytical process. XPS analysis was carried out on a VG Escalab Mark II spectrometry with CAE 50 eV and Mg Kα radiation.

3. Results and discussions

3.1. The synthesis of $Ca(AlH_4)_2$

The synthesis of calcium alanate by ball-milling the mixture of $2NaAlH_4 + CaCl_2$ was based on a metathesis reaction as follows:

$$2NaAlH_4 + CaCl_2 \rightarrow Ca(AlH_4)_2 + 2NaCl \quad (5)$$

The microstructures of as-synthesized samples at different ball-milling stages were characterized by XRD measurement. Fig. 1 shows the XRD patterns of the samples milled for 3–48 h. For comparison, the XRD pattern of mixed $2NaAlH_4 + CaCl_2$ sample that is hand-milled using an agate mortar and pestle for 5 min is also presented in Fig. 1. It can be seen that some diffraction peaks from $NaAlH_4$ and $CaCl_2$ disappear after ball milling for 3 h, the peak from NaCl emerges concurrently. $Ca(AlH_4)_2$ might be present in X-ray amorphous state initially, small diffraction peaks from $Ca(AlH_4)_2$ are found until the ball-milling time extends to 12 h, and are intensified with the increasing milling time. After milling for 48 h, the diffraction peaks of $NaAlH_4$ and $CaCl_2$ disappear completely, the product is a mixture of $Ca(AlH_4)_2$ and NaCl.

The characterization of $Ca(AlH_4)_2$ can also be performed by IR measurement. As it is known that the FTIR spectrum consists mainly of two wide bands, of which the ~1800 cm^{-1} band corresponds to the Al-H stretching vibrations. The characteristic band of Al-H bond changes with its chemical environment. Table 1 shows the frequencies (cm^{-1}) of $[AlH_4]^-$ group in different chemical environments. Combined with the spectra profile of the metathesis reaction product after ball-milling for 48 h shown in Fig. 2,

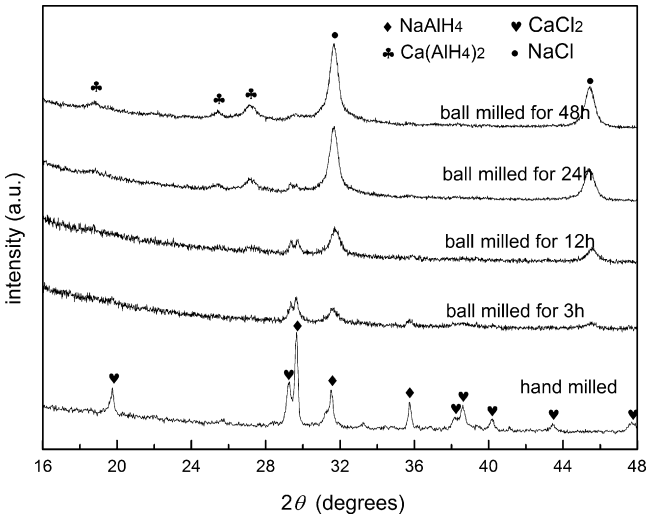

Fig. 1. XRD patterns of $2NaAlH_4 + CaCl_2$ samples milled for different milling times.

Table 1
The frequencies (cm^{-1}) of $[AlH_4]^-$ group in different chemical environments [8,10,22].

Complex	$Ca(AlH_4)_2$	$Mg(AlH_4)_2$	$NaAlH_4$	$KAlH_4$	$LiAlH_4$	
Frequencies	1798	1835	1675	1785	1757	1615

the results show that main contributions to the Al–H stretching vibrations are found at 1798 cm^{-1}. In the fingerprint, the band at 695 cm^{-1} is due to Ca–Al–H bending mode. The results from Fig. 2 together with Fig. 1 indicate that the reactants have transformed to $Ca(AlH_4)_2$ and NaCl after ball-milling for 48 h.

3.2. Dehydrogenation performance of the as-synthesized sample

The decomposition performance and desorbed hydrogen amount of the as-synthesized $Ca(AlH_4)_2 + 2NaCl$ sample milled for 48 h were studied by DSC/TG measurement (Fig. 3). It can be seen that the dissociation process of the as-synthesized sample is mainly divided into four stages (as reactions (1)–(4)).

The first step of decomposition is an exothermic process. DFT calculations indicated that the enthalpy value of the first step was −9 kJ/mol H_2 at the decomposition temperature of 127 °C [20]. TG

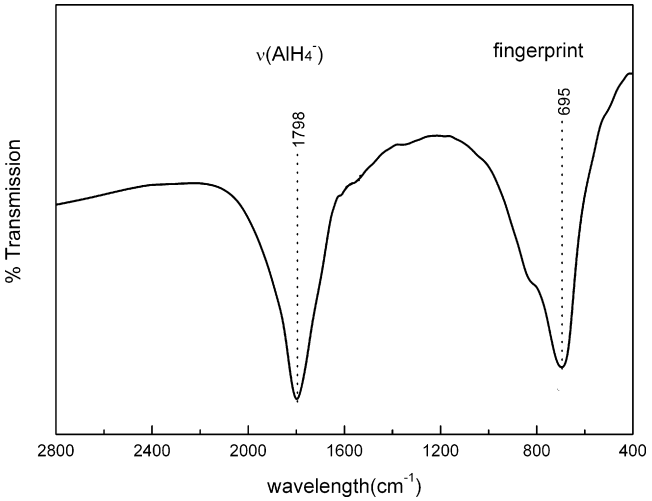

Fig. 2. FTIR spectra of the metathesis reaction product after ball-milling for 48 h, the band at 1798 cm^{-1} corresponds to the Al-H stretching vibrations.

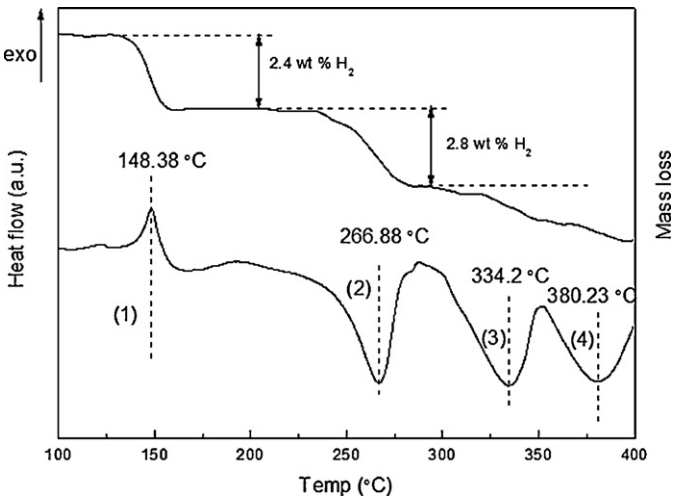

Fig. 3. DSC/TG curves of the as-synthesized $Ca(AlH_4)_2 + 2NaCl$ sample milled for 48 h at a heating rate of 10 °C/min.

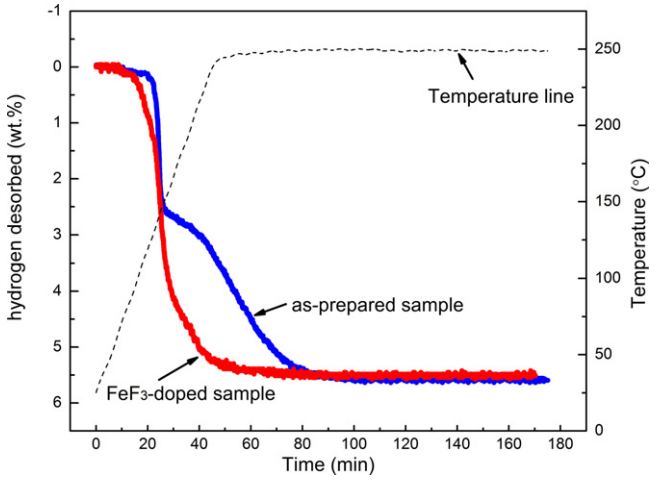

Fig. 5. TPD curves of the as-prepared and FeF_3-doped samples of $Ca(AlH_4)_2 + 2NaCl$ at a heating rate of 5 °C/min.

curve shows that the amount of released hydrogen is about 2.4 wt.%. The value is based on the ratio of the evaluated amount of desorbed hydrogen to the amount of $Ca(AlH_4)_2$ calculated from the reaction. The second step of decomposition begins at nearly 210 °C, corresponds to the decomposition of $CaAlH_5$ to CaH_2 and Al phase. $CaAlH_5$ is viewed as a promising on-board hydrogen storage reaction owing to its good thermodynamics (+32 kJ/mol H_2 according to the experimental value reported [11]). This step lasts until about 2.8 wt.% H_2 is desorbed. The last two steps involve the formation of Ca–Al alloys. According to the in situ XRD analysis reported [12], Al_4Ca formed first in the third step and a portion of it transferred to Al_2Ca in the fourth step. At 450 °C, the phase composition includes a mixture of Al_2Ca and Al_4Ca. The formation process of Ca–Al alloys needs higher temperature and is considered to be irreversible and impractical.

Fig. 4 shows the XRD patterns of the decomposition products of the as-synthesized $Ca(AlH_4)_2 + 2NaCl$ sample at different temperatures. It is shown that $CaAlH_5$ remains stable when heating to 200 °C, the pattern of $CaAlH_5$ is in good agreement with the Rietveld analysis results of Iosub et al. [15] and Weidenthaler et al. [19]. At 320 °C, $CaAlH_5$ is decomposed completely to CaH_2 and Al phases. After the temperature arises to 450 °C, the formed Ca–Al alloys mainly consist of Al_4Ca and Al_2Ca.

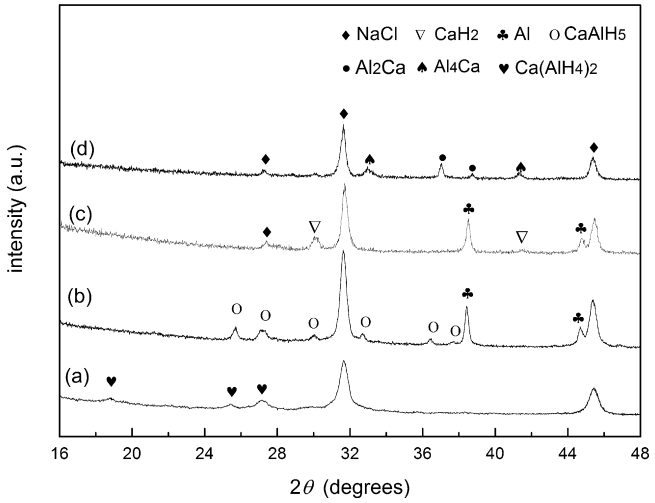

Fig. 4. XRD patterns of the decomposition products of the as-synthesized $Ca(AlH_4)_2 + 2NaCl$ sample when heating to different temperatures: (a) room temperature; (b) 200 °C; (c) 320 °C; (d) 450 °C.

The first two steps of the decomposition of $Ca(AlH_4)_2$ are considered for hydrogen storage application. However, the decomposition temperatures for reactions (1) and (2) are relatively high in comparison with the targeted value, and the thermolysis process of $Ca(AlH_4)_2$ and $CaAlH_5$ takes time. Therefore, it is necessary to find ways to improve the thermodynamic and kinetic properties of $Ca(AlH_4)_2$ system, clarify the main factors that controlling the behavior of dehydrogenation, which may contribute to the further understanding of thermodynamic and kinetic limitations in a number of high capacity complex hydrides.

3.3. *Influence of FeF_3 doping on the dehydrogenation performance of $Ca(AlH_4)_2$*

Fig. 5 records the courses of thermal dissociations of the as-prepared and FeF_3-doped samples of $Ca(AlH_4)_2 + 2NaCl$ by Sievert's apparatus. Samples are heated from room temperature to 250 °C at 5 °C/min. As evident from the figure, the starting point of decomposition for both is 70 °C, the difference is that FeF_3-doped sample experiences a shorter incubation stage before fast dehydrogenation. The temperature for fast-speed dehydriding is 90 °C for FeF_3-doped sample compared to 110 °C for the as-prepared sample. Besides, FeF_3-doped sample represents an obscure change in dehydrogenation kinetics that reflects the transition from reactions (1) to (2) when compared with the as-prepared sample, and the total time-consuming of the decomposition from $Ca(AlH_4)_2$ to CaH_2 has been shortened by about 30 min. The results suggests that FeF_3-doping is able to improve the dehydrogenation performance of $Ca(AlH_4)_2$ system effectively.

It is noteworthy that the desorbed hydrogen amount does not almost decline after 10 wt.% FeF_3 is doped. In Fig. 5, the desorbed hydrogen amounts of the as-prepared and FeF_3-doped samples are 5.5 and 5.48 wt.% respectively, in contrast with the theoretical hydrogen amount of 5.9 wt.%. The overflow of desorbed hydrogen might have been due to the reason that FeF_3 participates in the decomposition reactions, which brings additional hydrogen released.

In order to better understand the role of FeF_3 that improves the dehydrogenation performance, the thermal analyses were performed by the DSC methods. A series of measurements were conducted at different heating rates of 3, 5, 8 and 10 °C/min for the as-prepared and FeF_3-doped samples. According to the Kissinger

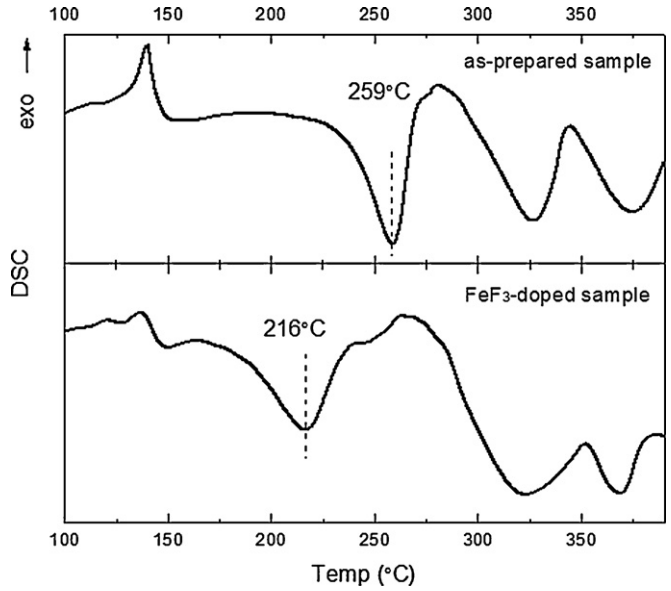

Fig. 6. DSC curves of the as-prepared and FeF_3-doped sample of $Ca(AlH_4)_2 + 2NaCl$ at a heating rate of 5 °C/min.

relation of reaction (6) [23]:

$$\ln\left(\frac{C}{T_p^2}\right) = -\frac{E_a}{RT_p} + A \quad (6)$$

where E_a is the activation energy for the transformation, R is the gas constant and A is a constant, C is heating rate and T_p is transformation peak temperature that changed with different heating rate (C), usually T_p shifts towards the higher temperature side with increasing heating rate. Fig. 6 shows the DSC curves of the as-prepared and FeF_3-doped sample at a heating rate of 5 °C/min. It is found that the decomposition process of FeF_3-doped sample remains four steps. In addition, the peak intensity for the first step changes and dissociation temperature of the second step is significantly dropped by about 43 °C compared with that of the as-prepared sample.

As is known that high temperature dehydrogenation mainly concentrates on the thermolysis of $CaAlH_5$ intermediate. In the above, FeF_3 doping makes for great reduction of decomposition temperature of $CaAlH_5$. In order to further understand the role of FeF_3 played on the dehydrogenation process of $CaAlH_5$, Fig. 7 gives the activation energies of $CaAlH_5$ decompositions calculated from the data performed at different heating rates (3, 5, 8 and 10 °C/min)

Table 2
Activation energy (E_a) of $CaAlH_5$, K_3AlH_6 and Na_3AlH_6.

Intermediate		E_a (kJ/mol)
$CaAlH_5$	As-prepared	161 [15], 153.4
	Doped	88.3
K_3AlH_6	As-prepared	131 ± 20 [8]
	Doped	105 ± 2 [8]
Na_3AlH_6	As-prepared	120 [24]
	Doped	97–100 [24]

for the as-prepared and FeF_3-doped samples. It is observed that the activation energy of the as-prepared sample is 153.4 kJ/mol, which is in good agreement with the published result in other literature [15]. With respect to the FeF_3-doped sample, the value of activation energy is 88.3 kJ/mol. The variation of activation energy poses an interesting approach to investigate the mechanism that hinders the dehydrogenation and rehydrogenation process.

It has been confirmed that $CaAlH_5$ is thermodynamically reversible by DSC analyses and DFT calculations, the reaction enthalpy of $CaAlH_5$ is 32 kJ/mol, which is in the targeted window suitable for near-ambient hydrogen storage [12,19,20]. However, the rehydrogenation of $CaAlH_5$ has not been realized experimentally due to its slow kinetics property. Table 2 lists the values of activation energy of some intermediates for comparison. It is interesting to see that the activation energy tends to be higher with the increasing of the size of metal cation. The value of $CaAlH_5$ is much higher than those of K_3AlH_6 and Na_3AlH_6 which are technically reversible [8,24], this indicates that mass transport is much more difficult in the dehydrogenation and rehydrogenation processes of $CaAlH_5$. Fortunately, FeF_3-doped sample exhibits favorable value compared to those of doped K_3AlH_6 and Na_3AlH_6. High activation energy may be the main factor that controlling the hydriding/dehydriding kinetics, and this result suggests a possibility to realize the rehydrogenation of $CaAlH_5$. However, rehydrogenation attempt under 100 bar H_2 and 160 °C for 24 h gave no sign of pressure change. It is suggested that unilateral kinetic enhancement is not enough for rehydriding. Further investigations about the improvements from thermodynamic and kinetic optimization of $CaAlH_5$ are underway.

3.4. The mechanism of FeF_3 doping for enhanced kinetics

To verify the structural changes during the dehydrogenation process of the FeF_3-doped sample of $Ca(AlH_4)_2 + 2NaCl$, and hence to understand the mechanism of FeF_3 doping for enhanced

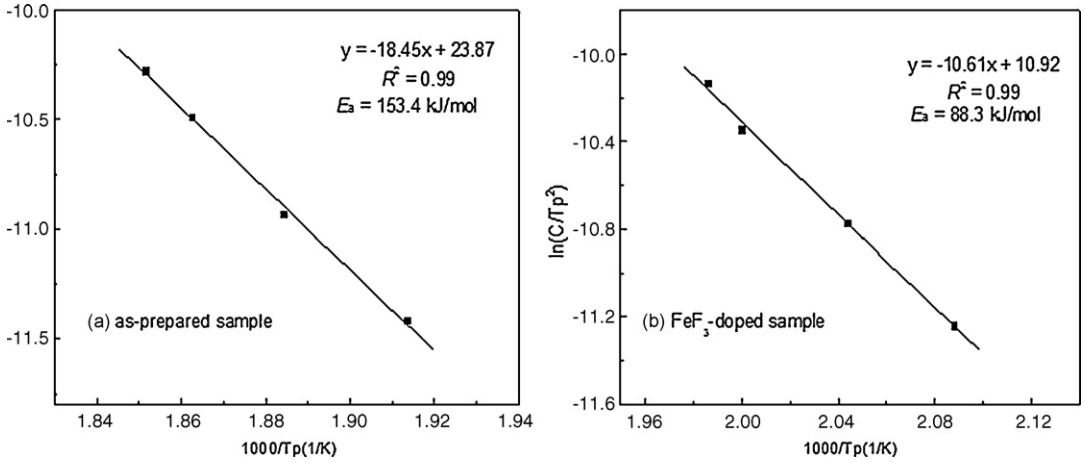

Fig. 7. Kissinger plots of $CaAlH_5$ decomposition reactions of the as-prepared (a) and FeF_3-doped (b) samples.

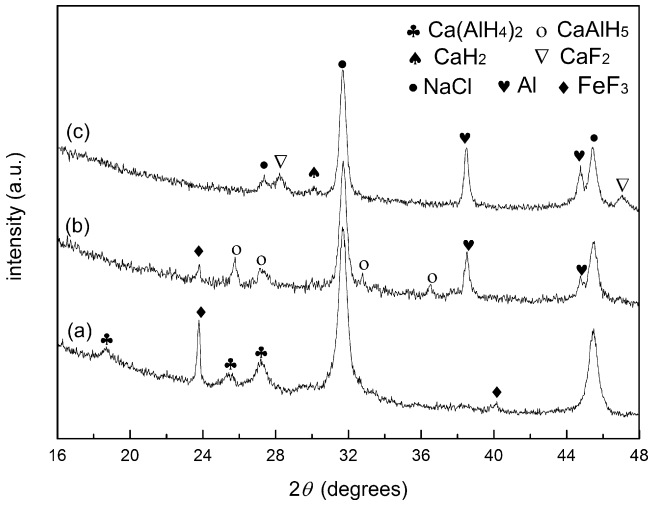

Fig. 8. XRD patterns of the decomposition products of the FeF_3-doped sample of $Ca(AlH_4)_2$ + 2NaCl at different decomposition temperatures: (a) room temperature; (b) 160 °C; (c) 250 °C.

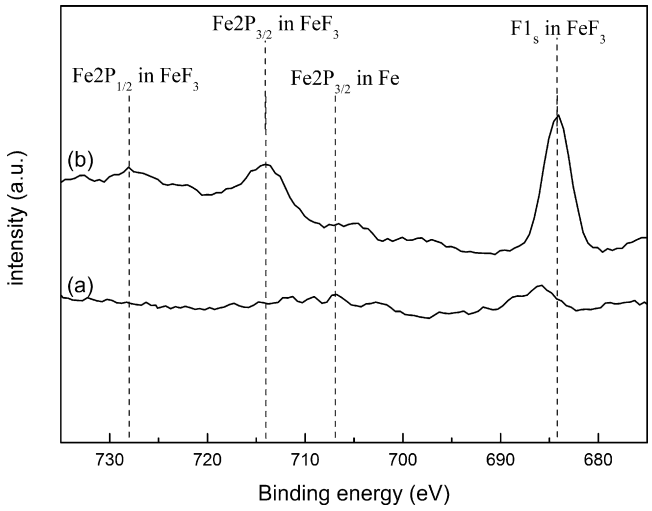

Fig. 9. XPS curves of (a) the decomposition products of FeF_3-doped sample at 250 °C and (b) commercial FeF_3.

dehydriding performance of $Ca(AlH_4)_2$ system, X-ray diffraction measurements were carried out. As shown in Fig. 8, when heating to 160 °C, $Ca(AlH_4)_2$ decomposes into $CaAlH_5$ and Al phases, FeF_3 is visible and no other fluoride is detected, which indicate that FeF_3 is stable during the first step decomposition reaction. At 320 °C, a new phase confirmed as CaF_2 appears following the disappearance of FeF_3. Based on XRD measurements and DSC analysis mentioned above, it can be conclude that FeF_3 might react with $CaAlH_5$ according to the following reaction:

$$CaAlH_5 + 2/3FeF_3 \rightarrow CaF_2 + 2/3Fe + Al + 5/2H_2 \quad (7)$$

The formation heats (ΔH_f), of CaF_2, FeF_3, and $CaAlH_5$ are −1228, 1042.3 and 31.6 kJ/mol, respectively [12,25], the total enthalpy change of reaction (7) is −501.5 kJ/mol. This indicates that reaction (7) is thermodynamically favorable. This result best explains the phenomenon reflected in Fig. 5 that desorbed hydrogen amount of $Ca(AlH_4)_2$ system does not almost decline after 10 wt.% FeF_3 is doped. The generation of CaF_2 leads to additional liberation of H_2, which allows the desorbed hydrogen amount changes in a limited range.

The absence of Fe phase in Fig. 8(c) is probably due to two reasons: First, the Fe phase is overlapped with the Al phase in XRD pattern, which induces that the characteristic peaks of Fe phase is obscured; Second, small amount of Fe phase might be highly-dispersed and in an extra fine form. However, the existence of Fe could be confirmed by XPS measurements. Fig. 9 shows the XPS spectra of the yields of reaction (7) as compared to the commercial FeF_3 powder. It can be observed that, when the reaction is completed, $Fe_{2p1/2}$, $Fe_{2p3/2}$ and F_{1s} peaks from FeF_3 disappear, a bulge region around 710 eV is visualized with a few peaks, of which the peak at 706.6 eV is attributed to $Fe_{2p3/2}$ in Fe, and the others are attributed to Fe oxides [26], which may be formed in the testing process. The weakness of peak intensity is probably duo to the reason that XPS spectra only detect the very limited penetration depth of the sample, in which very small amount of Fe disperses.

Reports about the improvement of hydriding/dehydriding properties by the intelligent manipulation of additional reactions exist in a great number [27,28]. It provides an available means to meet temperature and pressure requirements for complex hydrides as reversible hydrogen storage materials for mobile applications. In our work, the fluoride doping results in a substitution of H^- by F^- anion in the hydride lattice and hence probably a favorable thermodynamics adjustment, F^- acts as a functional anion [29]. Besides, the generated transitional metal Fe, like other transition-metal additives such as Ti or Ce, might be responsible for the improved kinetics of dehydrogenation. It is generally accepted that mass transport is the rate-limiting step during the decomposition of alanates, and dehydriding kinetics should be controlled by the diffusion of some species [30–32]. Hence, the highly dispersed transition-metal Fe might act as active catalyst to facilitate the diffusion process and dehydrogenation reaction.

4. Conclusions

The synthesis and characterization of $Ca(AlH_4)_2$ were investigated. The thermolysis of $Ca(AlH_4)_2$ involves four steps, of which the first two steps have a total amount of 5.2 wt.% desorbed hydrogen. $CaAlH_5$ as an important intermediate, has moderate decomposition enthalpy (+32 kJ/mol) and a theoretical gravimetric density of 4.2 wt.%, and is thought to be a promising near-ambient hydrogen storage material, but the decomposition of $CaAlH_5$ to CaH_2 begins at nearly 210 °C and its re-hydrogenation is still a challenge though DSC analysis and thermodynamic data have shown this possibility. The FeF_3-doped $Ca(AlH_4)_2$ exhibits similar thermolysis process except for significant reduction of dehydrogenation temperature (~43 °C) and activation energy (~65 kJ/mol) for the decomposition of $CaAlH_5$, making it perhaps a realized reversible hydrogen storage material that needs to be confirmed in following works. At last, the mechanism of FeF_3 doping for the enhanced dehydrogenation performance of $Ca(AlH_4)_2$ system has been discussed. Plausible reasons include the reaction of $CaAlH_5$ and FeF_3, and the catalyst effects are rendered by the generated CaF_2 and transitional metal Fe catalyst.

Acknowledgments

This work was financially supported by the National Basic Research Program of China under grant no. 2007CB209701 and 2010CB631300, the National Natural Science Foundation of China under grant no. 50871099 and 50631020, the China Postdoctoral Science Foundation under grant no. 200902622, the Program for New Century Excellent Talents in University under grant no. NCET-07-0741, and the University Doctoral Foundation of the Ministry of Education under grant no. 20090101110050.

References

[1] B. Bogdanovic, M. Schwickardi, J. Alloys Compd. 253–254 (1997) 1–9.
[2] X.Z. Ke, I. Tanaka, Phys. Rev. B 71 (2005) 024117.
[3] B. Bogdanovic, M. Felderhoff, A. Pommerin, F. Schüth, N. Spielkamp, Adv. Mater. 18 (2006) 1198–1201.
[4] C.P. Blade, B.P.C. Herijgers, J.H. Bitter, K.P. de Jong, J. Am. Chem. Soc. 130 (2008) 6761–6765.
[5] T. Sun, B. Zhou, H. Wang, M. Zhu, Int. J. Hydrogen Energy 33 (2008) 2260–2267.
[6] M. Resan, M.D. Hampton, J.K. Lomness, D.K. Slattery, Int. J. Hydrogen Energy 30 (2005) 1413–1416.
[7] F.H. Wang, Y.F. Liu, M.X. Gao, K. Luo, H.G. Pan, Q.D. Wang, J. Phys. Chem. C 113 (2009) 7978–7984.
[8] J.R. Ares, K.F. Aguey-Zinsou, F. Leardini, I.J. Ferrer, J.F. Fernandez, Z.X. Guo, C. Sánchez, J. Phys. Chem. C 113 (2009) 6845–6851.
[9] M. Mamatha, C. Weidenthaler, A. Pommerin, M. Felderhoff, F. Schüth, J. Alloys Compd. 416 (2006) 303–314.
[10] W. Schwab, K. Wintersberger, Z. Fur Naturforsch. Sect. B: J. Chem. Sci. 8 (1953) 690–691.
[11] M. Fichtner, C. Frommen, O. Fuhr, Inorg. Chem. 44 (2005) 3479–3484.
[12] A. Mamatha, B. Bogdanovic, M. Felderhoff, A. Pommerin, W. Schmidt, F. Schüth, J. Alloys Compd. 407 (2006) 78–86.
[13] K. Komiya, N. Morisaku, Y. Shinzato, K. Ikeda, S. Orimo, Y. Ohki, et al., J. Alloys Compd. 446 (2007) 237–241.
[14] H. Kabbour, C.C. Ahn, S.J. Hwang, R.C. Bowman Jr., J. Graetz, J. Alloys Compd. 446 (2007) 264–266.
[15] V. Iosub, T. Matsunaga, K. Tange, M. Ishikiriyama, Int. J. Hydrogen Energy 34 (2009) 906–912.
[16] Q.A. Zhang, E. Akiba, J. Alloys Compd. 460 (2008) 272–275.
[17] X.F. Liu, K. Asano, K. Sakaki, Y. Nakamura, H. Enoki, E. Akiba, J. Phys. Chem. C 112 (2008) 17423–17426.
[18] O.M. Lovvik, Phys. Rev. B 71 (2005) 144111.
[19] C. Weidenthaler, T.J. Frankcombe, M. Felderhoff, Inorg. Chem. 45 (2006) 3849–3851.
[20] C. Wolverton, V. Ozolins, Phys. Rev. B 75 (2007) 064101.
[21] T. Sato, M.H. Sorby, K. Ikeda, S. Sato, B.C. Hauback, S. Orimo, J. Alloys Compd. 487 (2009) 472–478.
[22] J.R. Fernandez, A.F. Aguey-Zinsou, M. Elsaesser, X.Z. Ma, M. Dornheim, T. Klassen, R. Bormann, Int. J. Hydrogen Energy 32 (2007) 1033–1040.
[23] H.E. Kissenger, Anal. Chem. 29 (1957) 1702–1706.
[24] M. Monteferrante, S. Bonella, S. Meloni, E. Vanden-Eijnden, G. Ciccotti, Sci. Model. Simul. 15 (2008) 187–206.
[25] D.R. Lide, CRC Handbook of Chemistry and Physics, 89th ed., CRC Press/Taylor and Francis, Boca Raton (internet version 2009).
[26] T. Yamashita, P. Hayes, Appl. Surf. Sci. 254 (2008) 2441–2449.
[27] J.J. Vajo, F. Mertens, C.C. Ahn, R.C. Bowman, B. Fultz, J. Phys. Chem. B 108 (2004) 13977–13983.
[28] X.L. Fan, X.Z. Xiao, L.X. Chen, K.R. Yu, Z. Wu, S.Q. Li, Q.D. Wang, Chem. Commun. 44 (2009) 6857–6859.
[29] L.C. Yin, P. Wang, X.D. Kang, C.H. Sun, H.M. Chen, Phys. Chem. Chem. Phys. 9 (2007) 1499–1502.
[30] D. Blanchard, H.W. Brinks, B.C. Hauback, J. Alloys Compd. 416 (2006) 72–79.
[31] A. Peles, C.G. Van de, Walle, Phys. Rev. B 76 (2007) 214101.
[32] H. Gunaydin, K.N. Houk, V. Ozoliņš, Proc. Natl. Acad. Sci. U.S.A. 105 (2008) 3673–3677.